Inorganic Chemistry
Article

Inorg. Chem. **2011**, *50*, 1135–1149 **1135**
DOI: 10.1021/ic102209q

Near-Infrared-Emitting Phthalocyanines. A Combined Experimental and Density Functional Theory Study of the Structural, Optical, and Photophysical Properties of Pd(II) and Pt(II) α-Butoxyphthalocyanines

Alexandra V. Soldatova,[†,⊥] Junhwan Kim,[‡] Corrado Rizzoli,[§] Malcolm E. Kenney,[‡] Michael A. J. Rodgers,[†] Angela Rosa,*[,∥] and Giampaolo Ricciardi*[,∥]

[†]*Center for Photochemical Sciences and Department of Chemistry, Bowling Green State University, Bowling Green, Ohio 43403, United States,* [‡]*Department of Chemistry, Case Western Reserve University, Cleveland, Ohio 44106, United States,* [§]*Dipartimento di Chimica Generale ed Inorganica, Università di Parma, Viale delle Scienze, 43100 Parma, Italy, and* [∥]*Dipartimento di Chimica, Università della Basilicata, Viale dell'Ateneo Lucano 10, 85100 Potenza, Italy.* [⊥]*Present address: Department of Chemistry, University of Washington, Seattle, WA 98195*

Received November 3, 2010

The structural, optical, and photophysical properties of 1,4,8,11,15,18,22,25-octabutoxyphthalocyaninato-palladium-(II), $PdPc(OBu)_8$, and the newly synthesized platinum analogue $PtPc(OBu)_8$ are investigated combining X-ray crystallography, static and transient absorption spectroscopy, and relativistic zeroth-order regular approximation (ZORA) Density Functional Theory (DFT)/Time Dependent DFT (TDDFT) calculations where spin−orbit coupling (SOC) effects are explicitly considered. The results are compared to those previously reported for $NiPc(OBu)_8$ (*J. Phys. Chem. A* **2005**, *109*, 2078) in an effort to highlight the effect of the central metal on the structural and photophysical properties of the group 10 transition metal octabutoxyphthalocyanines. Different from the nickel analogue, $PdPc(OBu)_8$ and $PtPc(OBu)_8$ show a modest and irregular saddling distortion of the macrocycle, but share with the first member of the group similar UV−vis spectra, with the deep red and intense Q-band absorption experiencing a blue shift down the group, as observed in virtually all tetrapyrrolic complexes of this triad. The blue shift of the Q-band along the $MPc(OBu)_8$ (M = Ni, Pd, Pt) series is interpreted on the basis of the metal-induced electronic structure changes. Besides the intense deep red absorption, the title complexes exhibit a distinct near-infrared (NIR) absorption due to a transition to the double-group 1E (π,π^*) state, which is dominated by the lowest single-group ^{3}E (π,π^*) state. Unlike $NiPc(OBu)_8$, which is nonluminescent, $PdPc(OBu)_8$ and $PtPc(OBu)_8$ show both deep red fluorescence emission and NIR phosphorescence emission. Transient absorption experiments and relativistic spin−orbit TDDFT calculations consistently indicate that fluorescence and phosphorescence emissions occur from the $S_1(\pi,\pi^*)$ and $T_1(\pi,\pi^*)$ states, respectively, the latter being directly populated from the former, and the triplet state decays directly to the S_0 surface (the triplet lifetime in deaerated benzene solution was 3.04 μs for Pd and 0.55 μs for Pt). Owing to their triplet properties, $PdPc(OBu)_8$ and $PtPc(OBu)_8$ have potential for use in photodynamic therapy (PDT) and are potential candidates for NIR light emitting diodes or NIR emitting probes.

Introduction

Metallophthalocyanines (MPcs) have found diverse applications[1] as a result of the inherent chemical flexibility of the metallomacrocycle, which allows modulation of their physicochemical properties through modification of the macrocycle and the coordinated metal. Introduction of butoxy groups at the α-positions of the Pc macrocycle to yield α-butoxymetallophthalocyanines, $MPc(OBu)_8$,[2−6] greatly enhances the solubility of MPcs in common organic solvents, enables out-of-plane distortions of the macrocycle,[6,7] and, most

*To whom correspondence should be addressed. E-mail: angela.rosa@unibas.it (A.R.); rg010sci@unibas.it (G.R.).

(1) *Phthalocyanines: Properties and Applications*; Leznoff, C. C.; Lever, A. B. P., Eds.; VCH Publishers: New York, 1990−1996; Vol. *1*−*4*.
(2) Cook, M. J.; Dunn, A. J.; Howe, S. D.; Thomson, A. J.; Harrison, K. J. *J. Chem. Soc., Perkin Trans.* **1988**, *1*, 2453.
(3) Rihter, B. D.; Kenney, M. E.; Ford, W. E.; Rodgers, M. A. J. *J. Am. Chem. Soc.* **1990**, *112*, 8064.
(4) Kobayashi, N.; Ogata, H.; Nonaka, N.; Luk'yanets, E. A. *Chem.—Eur. J.* **2003**, *9*, 5123.
(5) Miwa, H.; Ishii, K.; Kobayashi, N. *Chem.—Eur. J.* **2004**, *10*, 4422.
(6) Gunaratne, T. C.; Gusev, A. V.; Peng, X.; Rosa, A.; Ricciardi, G.; Baerends, E. J.; Rizzoli, C.; Kenney, M. E.; Rodgers, M. A. J. *J. Phys. Chem. A* **2005**, *109*, 2078.
(7) Gao, Y.; Chen, Y.; Li, R.; Bian, Y.; Li, X.; Jiang, J. *Chem.—Eur. J.* **2009**, *15*, 13241.

Published on Web 12/28/2010

importantly, induces a red-shift of the Q-band system by more than 60 nm.[2−6] Owing to the intense absorptions in the red to deep red region, which coincides with the therapeutic window where tissue absorption and scattering is minimal, $MPc(OBu)_8$s have been shown to have potential for applications in photomedicine as it relates to cancer treatments such as photothermal therapy (PTT) and photodynamic therapy (PDT).[3,6] The coordinated metal plays a central role in determining the excited state dynamics of the $MPc(OBu)_8$ complexes, and hence their suitability as PDT or PTT photosensitizers, the first two members of the group 10 transition metal α-butoxyphthalocyanines, $NiPc(OBu)_8$ and $PdPc(OBu)_8$, providing an instructive example. A combined experimental and theoretical investigation of the photophysics of $NiPc(OBu)_8$ has shown that this compound meets the conditions for a photothermal process to be effective.[6] In $NiPc(OBu)_8$ the primarily excited $S_1(\pi,\pi^*)$ state rapidly (640 ps) deactivates via lower-lying ^{3}(d,d) and ^{3}LMCT (π,d) states generating a vibrationally hot ground state molecule and hence producing highly localized thermal effects that can eventually lead to cell death. At variance with $NiPc(OBu)_8$, $PdPc(OBu)_8$ is emissive. Previous photophysical studies have shown that this compound is a powerful photogenerator of O_2 ($^1\Delta_g$) and hence a promising PDT photosensitizer.[3] Because of the high photostability and triplet quantum yield (0.77), $PdPc(OBu)_8$ has been recently used also as a triplet sensitizer in triplet−triplet annhilation from rubrene, which makes this phthalocyanine well suited for applications in non-linear optics.[8]

Although the triplet state of $PdPc(OBu)_8$ has been well characterized,[3] neither experimental studies on the excited state dynamics nor theoretical analysis of the nature and energy of the lowest excited states have been reported so far. Moreover, the photoproperties of $PtPc(OBu)_8$ are still unknown, mainly because of the lack of an efficient synthetic path to this complex. In an effort to highlight the effect of the central metal on the photoproperties of the group 10 transition metal α-butoxyphthalocyanines, the static and dynamic photophysical properties of $PdPc(OBu)_8$ and of the newly synthesized $PtPc(OBu)_8$ complexes are investigated in depth and compared to those previously reported for the nickel analogue.[6] The complexes have been structurally characterized through single crystal X-ray analysis, and their optical and photophysical properties have been interpreted with the aid of density functional theory (DFT)[9,10] and time-dependent DFT (TDDFT)[11,12] calculations of the ground and excited states. Scalar relativistic effects on the ground and excited states were considered using the DFT/TDDFT zeroth-order regular approximation (ZORA) formalism.[13−15] Spin−orbit coupling effects on the excited states, which are relevant to estimate coupling between states of different multiplicities and hence to explain the intersystem crossing (ISC) processes and phosphorescence, were evaluated using the approximate spin−orbit (ASO)-ZORA TDDFT[16] formalism recently implemented in the Amsterdam Density Functional (ADF) program package.[17−19]

Experimental Section

Synthesis. $PdPc(OBu)_8$. A mixture of $H_2Pc(OBu)_8$ (81 mg, 0.075 mmol) and $PdCl_2$ (40 mg, 0.23 mmol) and dimethylformamide (3 mL) was stirred at 120 °C for 24 h and evaporated to dryness by rotary evaporation (40 °C). The solid was treated with pyridine (20 mL) for 2 h, and the solution was chromatographed three times (Al_2O_3 III, pyridine; Al_2O_3 III, pyridine-toluene, 1:3; Al_2O_3 III, $CHCl_3$), vacuum-dried (room temperature) and weighed (65 mg, 73%). UV−vis (toluene): λ_{max}, nm (log ε): 722 nm (5.6). NMR ($CDCl_3$): δ 7.58 (s, 8H, 2,3-Ar H), 4.89 (t, 16H, OCH_2), 2.25 (m, 16H, OCH_2CH_2), 1.67 (m, 16H, $OCH_2CH_2CH_2$), 1.10 (t, 24H, $OCH_2CH_2CH_2CH_3$). HRMS-ESI-TOF (m/z): $(M+H)^+$ calcd for $C_{64}H_{81}N_8O_8{}^{106}Pd$, 1195.5234; found, 1195.5149.

The compound is a green solid. It is soluble in CH_2Cl_2 and toluene and slightly soluble in dimethyformamide and hexanes.

$PtPc(OBu)_8$. A mixture of $H_2Pc(OBu)_8$ (108 mg, 0.10 mmol) and $PtCl_2$ (76 mg, 0.30 mmol) and dimethylformamide (3 mL) was stirred at 100 °C for 20 h and evaporated to dryness by rotary evaporation (40 °C). The solid was chromatographed three times (Al_2O_3 III, pyridine-toluene, 9:1; Al_2O_3 III, pyridine-toluene, 1:3; Al_2O_3 III, $CHCl_3$), vacuum-dried (room temperature) and weighed (56 mg, 44%). UV−vis (toluene): λ_{max}, nm (log ε): 711 nm (5.7). NMR ($CDCl_3$): δ 7.55 (s, 8H, 2,3-Ar H), 4.88 (t, 16H, OCH_2), 2.24 (m, 16H, OCH_2CH_2), 1.67 (m, 16H, $OCH_2CH_2CH_2$), 1.10 (t, 24H, $OCH_2CH_2CH_2CH_3$). HRMS-ESI-TOF (m/z): $(M+H)^+$ calcd for $C_{64}H_{81}N_8O_8{}^{195}Pt$, 1284.5830; found, 1284.5807.

The compound is a green solid. It is soluble in CH_2Cl_2 and toluene and slightly soluble in dimethylformamide and hexanes.

X-ray Crystallographic Data Collection and Refinement of the Structures. X-ray intensities for $PdPc(OBu)_8$ and $PtPc(OBu)_8$ were collected on a Bruker SMART 100 CCD diffractometer equipped with Mo Kα radiation (λ = 0.71073 Å) at 295(2) and 293(2) K, respectively.

Absorption corrections were applied using SADABS.[20] The structures were solved by direct methods using SIR97[21] and refined by full-matrix least-squares on F^2 using the SHELXL-97 program.[22] All the non-hydrogen, except for the disordered carbon atoms, were refined anisotropically. The H atoms were positioned geometrically and refined using a riding model [C−H = 0.93−0.97 Å] with $U_{iso}(H) = 1.2U_{eq}(C)$. In the $PdPc(OBu)_8$ complex some butyl chains were affected by rather high displacement parameters indicating the presence of disorder. The best fit was found by splitting the disordered carbon atoms over two positions (called A and B) with site occupation factors of 0.5/0.5 for C50, C51, C52 and 0.7/0.3 for C59, C60. In the $PtPc(OBu)_8$ complex, all but one butyl chains were affected by severe disorder, which was solved by splitting the disordered

(8) Singh-Rachford, T.; Castellano, F. N. *J. Phys. Chem. A* **2008**, *112*, 3550.
(9) Parr, R. G.; Yang, W. *Density Functional Theory of Atoms and Molecules*; Oxford University Press: New York, 1989.
(10) Parr, R. G.; Yang, W. *Annu. Rev. Phys. Chem.* **1995**, *46*, 701.
(11) Drew, A.; Head-Gordon, M. *Chem. Rev.* **2005**, *105*, 4009.
(12) Casida, M. E. In *Recent Advances in Density Functional Methods*; Chong, D. P., Ed.; World Scientific: Singapore, 1995; Vol. *1*; p 155.
(13) Van Lenthe, E.; Baerends, E. J.; Snijders, J. G. *J. Chem. Phys.* **1993**, *99*, 4597.
(14) Van Lenthe, E.; Baerends, E. J.; Snijders, J. G. *J. Chem. Phys.* **1994**, *101*, 9783.
(15) Van Lenthe, E.; Ehlers, A. W.; Baerends, E. J. *J. Chem. Phys.* **1999**, *110*, 8543.
(16) Wang, F.; Ziegler, T. *J. Chem. Phys.* **2005**, *123*, 154102.
(17) Fonseca Guerra, C.; Snijders, J. G.; Te Velde, G.; Baerends, E. J. *Theor. Chem. Acc.* **1998**, *99*, 391.
(18) *ADF2009.01*; SCM, Theoretical Chemistry, Vrije Universiteit: Amsterdam, The Netherlands, 2009; http://www.scm.com.
(19) Te Velde, G.; Bickelhaupt, F. M.; Baerends, E. J.; Fonseca Guerra, C.; Van Gisbergen, S. J. A.; Snijders, J. G.; Ziegler, T. *J. Comput. Chem.* **2001**, *22*, 931.
(20) *SMART, SAINT-Plus, and SADABS*; Bruker Axs Inc.: Madison, WI, 1998.
(21) Altomare, A.; Burla, M. C.; Camalli, M.; Cascarano, G.; Giacovazzo, C.; Guagliardi, A.; Moliterni, A. G. G.; Polidori, G.; Spagna, R. *J. Appl. Crystallogr.* **1999**, *32*, 115.
(22) Sheldrick, G. M. *Acta Crystallogr.* **2008**, *A64*, 112.

Table 1. Crystallographic Data for $PdPc(OBu)_8$ and $PtPc(OBu)_8$

	$PdPc(OBu)_8$	$PtPc(OBu)_8$
formula	$C_{64}H_{80}N_8O_8Pd$	$C_{64}H_{80}N_8O_8Pt$
data coll. T, K	295(2)	293(2)
crystal color	dark green	dark green
crystal size (mm^3)	$0.15 \times 0.22 \times 0.28$	$0.18 \times 0.21 \times 0.37$
formula weight	1195.8	1284.5
crystallographic system	monoclinic	monoclinic
space group	$P2_1/c$	$P2_1/c$
a, Å	18.841(2)	13.931(2)
b, Å	18.776(2)	16.028(2)
c, Å	17.500(2)	28.318(2)
β, deg	95.581(2)	99.317(2)
V, $Å^3$	6161.4(12)	6239.6(14)
Z	4	4
density (calcd, g cm^{-3})	1.289	1.367
absorption coefficient (mm^{-1})	0.361	2.308
$F(000)$	2520	2648
collected reflections	64998	39177
independent reflections	13784	9011
observed reflections	6598	4377
parameters	725	670
GOF on F^2	1.036	0.845
R, wR_2 [$I > 2\sigma(I)$]	0.051, 0.094	0.044, 0.064
R, wR_2 (all data)	0.144, 0.109	0.115, 0.070
largest difference peak and hole (e $Å^{-3}$)	0.90, −0.31	0.88, −0.43

atoms over two positions (positions A and B) with site occupation factors fixed at 0.5/0.5 for C33−C36, C46−C48, 0.6/0.4 for C42−C44, C61−C64, and 0.7/0.3 for O7, C50−C60. During the refinement, the 1−2 and 1−3 C−C bond distances within the disordered chains were constrained to be 1.54(1) and 2.52(3) Å, respectively. In $PtPc(OBu)_8$ the benzene rings of the phthalocyanine macrocycle were refined as regular hexagons. Crystallographic data and other pertinent information are summarized in Table 1. Selected bond distances and angles are reported in Tables S1 and S2 in the Supporting Information. Additional details on the crystallographic study as well as atomic displacement parameters are given as as a CIF file in the Supporting Information.

UV−vis and NIR Absorption Spectra. The ground state electronic absorption spectra were recorded at room temperature on a Varian Cary 50 Bio (Varian Corporation) UV−visible single beam spectrophotometer using 10 mm or 2 mm path length quartz cuvette. The near-IR (NIR) spectra were recorded using a Varian Cary 500E UV−vis−NIR absorption spectrophotometer. In each measurement the sample was referenced to a matched cuvette containing pure solvent. To observe optically forbidden transitions in the NIR region, samples with concentration of about 1.7 mM were employed. No aggregation phenomena were observed under such condition.

Fluorescence Spectra. Fluorescence spectra were obtained using a single photon counting spectrofluorimeter with a 450 W Xe lamp (340 nm) from Edinburgh Analytical Instruments (FL/FS 900). The luminescence signal was detected with a Peltier-cooled (−30 °C), R955 red-sensitive photomultiplier tube (PMT).

The fluorescence quantum yields were measured using $GePc(OSi(n\text{-}C_6H_{13})_3)_2$ in toluene as a standard ($\Phi_F = 0.6$).[23] The reference and the samples were excited at 645 nm where they had the same absorbance ($A = 0.03$ au). The areas under the fluorescence spectra (G) were measured and fluorescence quantum yields were calculated according to the expression:

$$\Phi_F^{sample} = \frac{G_{sample} A_{GePc}}{A_{sample} G_{GePc}} \Phi_F^{GePc}$$

All solutions were air saturated.

Phosphorescence Spectra. The steady-state phosphorescence spectra were measured at room temperature with a home-built spectrophotometer described elsewhere.[24] A liquid-nitrogen-cooled germanium detector and preamplifier were used to monitor the NIR signals. Samples in a 10 mm × 10 mm path length quartz cuvette were excited at 488 nm with light from a cw Ar ion laser (Coherent). Solutions were Ar-saturated.

Ultrafast Pump−Probe Measurements. The pump−probe instrument for ultrafast transient absorption measurements available in the Ohio Laboratory for Kinetic Spectrometry was employed to characterize the excited state deactivation of the studied compounds.[23,25] In the current experiments, the excitation wavelength at 650 nm was generated with an optical parametric amplifier (OPA 800C, Spectra Physics), pumped with 800 nm light from an amplified, mode-locked Ti:Sapphire laser (Hurricane, Spectra Physics). The transient absorption signal was monitored with a white light continuum probe, generated by focusing the 7% of the 800 nm fundamental into a 3 mm sapphire plate. Prior to continuum generation, the 800 nm beam went to a computer-controlled optical delay stage (MM 4000, Newport Corporation) that provided an experimental time window of about 1.6 ns with a step resolution of 6.6 fs. The linear polarization of the pump beam was set at an angle of 54.7° with respect to that of the probe beam to eliminate the influence of molecular reorientation on the observed dynamics. The instrument rise time of the ultrafast spectrometer was about 130 fs. Typical pump energy at the sample was 1 μJ per pulse. The sample flow-through cell had an optical path of 2 mm and was connected to a solution reservoir and flow system. The concentrations of the phthalocyanines were typically 22 μM. The absorption spectra of the solutions were measured before and after the experiment to check for possible sample degradation.

Nanosecond Transient Absorption Measurements. Experiments on the supra-nanosecond time scale were performed with a Q-switched Nd:YAG laser (Spectra Physics Quanta Ray GCR-230) and a computer aided kinetic spectrometer, described elsewhere.[3,23,25] The laser operated in the frequency tripled mode at 355 nm (6 ns, 10 Hz). To obtain transient absorption spectra, benzene solutions were Ar-saturated prior to the experiment. The concentrations of the samples were about 6 μM providing $A_{355} = 0.1$ in a 10 mm cuvette. To measure the oxygen quenching rate constant the kinetic profiles were taken in Ar, air, and O_2 saturated solutions. The oxygen concentration in the solution was calculated using the values of solubility of oxygen in benzene from ref 26.

Triplet Extinction Coefficients and Quantum Yield. The relative actinometry method was used to measure the product $\Phi_T \Delta\varepsilon_T$. $PdPc(OBu)_8$ was used as a reference with literature value for Φ_T of 0.77.[3] The samples in benzene were prepared with matched absorption of 0.09 at 355 nm in 10 mm path length cuvettes. Values of ΔA_{650} were recorded immediate postpulse prior to any decay occurring in Ar-saturated benzene. These numbers were used to calculate the triplet state quantum yield for Pt phthalocyanine:

$$\Phi_T^{PtPc} \times \Delta\varepsilon_T^{PtPc}(620) = \frac{\Delta A_{620}^{PtPc}}{\Delta A_{620}^{PdPc}} \times \Phi_T^{PdPc} \times \Delta\varepsilon_T^{PdPc}(620)$$

The total depletion method[27] was used to obtain the triplet-minus-ground state extinction coefficients, $\Delta\varepsilon_T$, at 620 nm, for both compounds. The coefficients obtained with this procedure

(23) Pelliccioli, A. P.; Henbest, K.; Kwag, G.; Carvagno, T. R.; Kenney, M. E.; Rodgers, M. A. J. *J. Phys. Chem. A* **2001**, *105*, 1757.

(24) Firey, P. A.; Ford, W. E.; Sounik, J. R.; Kenney, M. E.; Rodgers, M. A. J. *J. Am. Chem. Soc.* **1988**, *110*, 7626.

(25) Nikolaitchik, A. V.; Korth, O.; Rodgers, M. A. J. *J. Phys. Chem. A* **1999**, *103*, 7587.

(26) Murov, S. L.; Carmichael, I.; Hug, G. L. *Handbook of Photochemistry*; Marcel Dekker, Inc.: New York, 1993.

(27) Carmichael, I.; Hug, G. L. *J. Phys. Chem.* **1985**, *89*, 4036.

were $1.32 \times 10^4\ M^{-1}\ cm^{-1}$ and $1.16 \times 10^4\ M^{-1}\ cm^{-1}$ for the Pd and Pt complexes, respectively.

Quantum Chemical Calculations. The calculations were done with ADF[17−19] release 2009.01 as well as with Turbomole V6.1 packages.[28,29] The calculations were performed on the model compounds, $MPc(OMe)_8$ (M = Ni, Pd, Pt; Me = methyl), in which the butyl chains are replaced by methyl groups. The ground state and excited state geometries were optimized in vacuo with DFT[9,10] and its time-dependent variant, TDDFT,[11,12] respectively, employing the hybrid B3LYP[30−32] exchange-correlation (xc) functional and the def2-TZVP[33] basis set available in Turbomole. The 28 inner-core electrons of Pd and the 60 inner-core electrons of Pt were described by a relativistic Effective Core Potential (ECP), def2-ECP.[34] The ground and excited state geometries were confirmed to be energy minima by calculating the harmonic vibrational frequencies. Ground state single-point calculations were performed with ADF at the gas-phase equilibrium geometries obtained with Turbomole, using the hybrid B3LYP functional. For the palladium and platinum complexes the scalar relativistic (SR) ZORA formalism[13−15] was employed. For the nonrelativistic calculations on the Ni complex the all-electron TZP basis set was used, whereas for the SR-ZORA calculations on the Pd and Pt complexes the all-electron ZORA/TZP[35] basis set was used. The absorption spectra were computed at the equilibrium geometry of the electronic ground state, whereas fluorescence and phosphorescence spectra were computed at the equilibrium geometry of the lowest singlet and triplet excited states, respectively, using ADF. The vertical absorption energies and oscillator strengths of the nickel complex were computed at the TDDFT/B3LYP/TZP level of theory. The excitation energies (vertical absorption and vertical emission energies) and oscillator strengths of the palladium and platinum complexes were computed using both the SR-ZORA TDDFT[13−15] and the ASO-ZORA TDDFT[16] formalisms. In the ASO-ZORA TDDFT formalism, recently implemented in ADF for closed-shell systems, SR-ZORA TDDFT calculations are first performed to determine the lowest single-group excited states and the spin−orbit coupling operator is applied to these single-group excited states to obtain the excitation energies with spin−orbit coupling effects included. The computational effort of this method is much smaller than that of the two-component TDDFT formalism[36] and can be applied to large systems containing heavy elements. The composition of the double-group excited states in terms of the single-group singlet and triplet excited states are obtained automatically from the calculations. In the SR-ZORA and ASO-ZORA TDDFT calculations the hybrid B3LYP xc fuctional was employed in combination with the all-electron ZORA/TZP basis set.[35] Solvation effects on the ground state properties as well as on the excitation energies were evaluated using the conductor-like continuum solvent model (COSMO).[37,38]

Results and Discussion

A. Synthesis. The Pd and Pt compounds can be prepared by straightforward metal-insertion reactions in which the metal chlorides are used as the metal source:

$$MCl_2 + H_2Pc(OBu)_8 \rightarrow MPc(OBu)_8 \qquad (M = Pd, Pt)$$

The earlier preparation of $PdPc(OBu)_8$ with $PdCl_2(PPh_3)_2$ as the Pd source provides a precedent for these syntheses.[3] On the basis of the absence of $H_2Pc(OBu)_8$ in the $PtPc(OBu)_8$ reaction product, it appears that the relatively low yield of $PtPc(OBu)_8$ is caused by a Pt-catalyzed decomposition of $H_2Pc(OBu)_8$ during the synthesis.

B. X-ray Structure. A side-view of the X-ray molecular structure of the Pd and Pt complexes is shown in Figure 1. To highlight the structural characteristics of the macrocycles the ORTEP side-view of Figure 1 does not include the butyl chains. A top-view of the $PdPc(OBu)_8$ and $PtPc(OBu)_8$ molecular structures including the peripheral butyl groups and showing the numbering of all atoms is reported in Figures S1 and S2 of the Supporting Information, respectively. Selected bond distances and angles for the Pd and Pt complexes are quoted in Tables S1 and S2 of the Supporting Information, respectively. The structural data reveal that in both complexes the Pc macrocycle slightly deviates from planarity, mainly because of a sideway and/or vertical tilt of the indole moieties.

The sideway tilting (ruffling) of the indole rings is modest in both complexes. The average transannular torsion angle $(C_\alpha N_p N_p C_\alpha)_{op}$ and out-of-plane displacement of the meso nitrogen atoms from the phthalocyanine mean plane, $|\Delta N_{meso}|$, which are the appropriate descriptors of the ruffling distortions, are 3.0(3)° and 0.113(3) Å in the Pd complex, 2.6(9)° and 0.133(7) Å in the Pt complex.

At variance with the nickel analogue[6] where the macrocycle assumes a remarkable saddle conformation, with the indole rings tilted alternately up and down, almost as rigid bodies, $PdPc(OBu)_8$ and $PtPc(OBu)_8$ show a modest and less regular saddling distortion of the macrocycle with the vertical tilting varying significantly from an indole to another. The dihedral angles the indole rings form with the phthalocyanine mean plane, φ_{sad}, are 12.03(5)°, 1.64(4)°, 10.56(4)°, and 4.64(5)° in the Pd complex, 9.62(7)°, 8.81(11)°, 13.32(11)°, and 7.02(8)° in the heavier element analogue.

In $PdPc(OBu)_8$ and in $PtPc(OBu)_8$ even more, the out-of-plane displacement of the macrocycle mainly involves the benzene rings of the indoles, as the mean absolute perpendicular displacements of the N_p, C_α, C_β, C_o and C_m atoms from the phthalocyanine mean plane indicate. Actually, $|\Delta N_p|$, $|\Delta C_\alpha|$, $|\Delta C_\beta|$, $|\Delta C_o|$, and $|\Delta C_m|$ are 0.111(3), 0.105(3), 0.184(4), 0.271(4), and 0.406(4) Å in the Pd complex, 0.103(6), 0.134(9), 0.290(10), 0.487(10), and 0.679(10) Å in the Pt complex.

The $(N_p)_4$ core shows a small but not negligible tetrahedral distortion in both complexes, the displacement of the pyrrolic nitrogens from the $(N_p)_4$ mean plane ranging from −0.018(2) to 0.018(2) Å in the Pd complex, and from −0.039(6) to 0.038(6) Å in the Pt complex. The palladium and platinum atoms are displaced from the $(N_p)_4$ mean plane by 0.0222(2) and 0.0006(5) Å, respectively.

In $PdPc(OBu)_8$ the $M-N_p$ bond distances involving the N1 and N5 atoms (mean value 1.990(2) Å) are significantly

(28) *TURBOMOLE* V6.1 2009, a development of University of Karlsruhe and Forschungzentrum Karlsruhe GmbH, 1989−2007; TURBOMOLE GmbH, since 2007; available from http://www.turbomole.com.
(29) Ahlrichs, R.; Bär, M.; Häser, M.; Horn, H.; Kölmel, C. *Chem. Phys. Lett.* **1989**, *162*, 165.
(30) Becke, A. D. *J. Chem. Phys.* **1993**, *98*, 5648.
(31) Lee, C.; Yang, W.; Parr, R. G. *Phys. Rev. B* **1988**, *37*, 785.
(32) Stephens, P. J.; Devlin, F. J.; Chabalowski, C. F.; Frisch, M. J. *J. Phys. Chem.* **1994**, *98*, 11623.
(33) Weigend, F.; Ahlrichs, R. *Phys. Chem. Chem. Phys.* **2005**, *7*, 3297.
(34) Andrae, D.; Haeussermann, U.; Dolg, M.; Stoll, H.; Preuss, H. *Theor. Chim. Acta* **1990**, *77*, 123.
(35) Van Lenthe, E.; Baerends, E. J. *J. Comput. Chem.* **2003**, *24*, 1142.
(36) Wang, F.; Ziegler, T. *J. Chem. Phys.* **2005**, *123*, 194102.
(37) Klamt, A.; Schürmann, G. *J. Chem. Soc., Perkin Trans.* **1993**, *2*, 799.
(38) Klamt, A.; Jonas, V. *J. Chem. Phys.* **1996**, *105*, 9972.

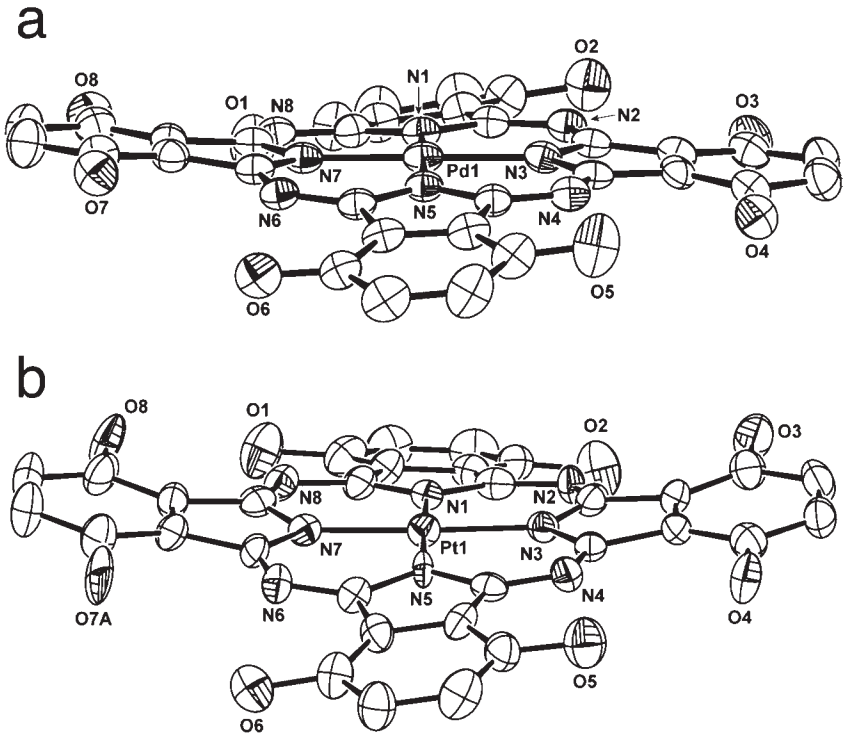

Figure 1. ORTEP side-view (30% probability ellipsoids) of (a) $PdPc(OBu)_8$ and (b) $PtPc(OBu)_8$. Butyl chains and hydrogen atoms have been omitted for clarity.

longer than those involving the N3 and N7 atoms (mean value 1.967(3) Å). These values compare well with the mean Pd−N_p distance of 1.974(2) Å reported for the [PdPc-$(OCHPr^i_2)_4$] complex.[39]

In $PtPc(OBu)_8$ the M−N_p bond distances involving the N1, N3, and N7 atoms are very similar to each other (mean value 1.959(6) Å) and remarkably longer than that involving the N5 atom (1.927(5) Å). Such a short Pt−N5 bond leads to a mean value of the Pt−N_p bond distance much smaller than that reported for the unsubstituted complex PtPc[40] (1.951(6) Å vs 1.980 Å). The different pattern of the M−N_p bond lengths in the Pd and Pt complexes reflects a quite different crystal packing (vide infra).

The C−N and C−C bond distances and angles within the macrocycles are consistent with a complete delocalization of the macrocycle π system. As observed in the analogous Ni compound, there is some conjugation between the oxygen lone pairs and the phthalocyanine π system, the mean values of the C_o−O bond distances being 1.370(5) Å and 1.371(12) Å (1.39(3) if the C_o−O7 bond distance is included in the average) in the Pd and Pt complexes, respectively. The extent of the π conjugation, however, depends significantly on the displacement of the C_{but} atoms from the plane of the corresponding benzene rings that ranges from 0.039(5) to 1.459(5) Å (mean value 0.838(5) Å) in the Pd complex and from 0.163(15) to 1.22(3) Å (mean value 0.84(3) Å) in the Pt analogue.

In the crystal structure of $PdPc(OBu)_8$, pairs of molecules (at x, y, z and $1-x$, $-y$, $-z$) partly overlap resulting in the formation of centrosymmetric dimers. The separation between the mean planes of the molecules in the dimer is 3.476(2) Å. The dimers pack along the c axis in a herringbone arrangement (Figure 2). Some C−H···O and C−H···N contacts involving the C atoms of the aliphatic chains could be interpreted as weak hydrogen interactions, the shortest one being: C39···$O7^i$, 3.494(6) Å; H391···$O7^i$, 2.55 Å; C39−H391···$O7^i$,

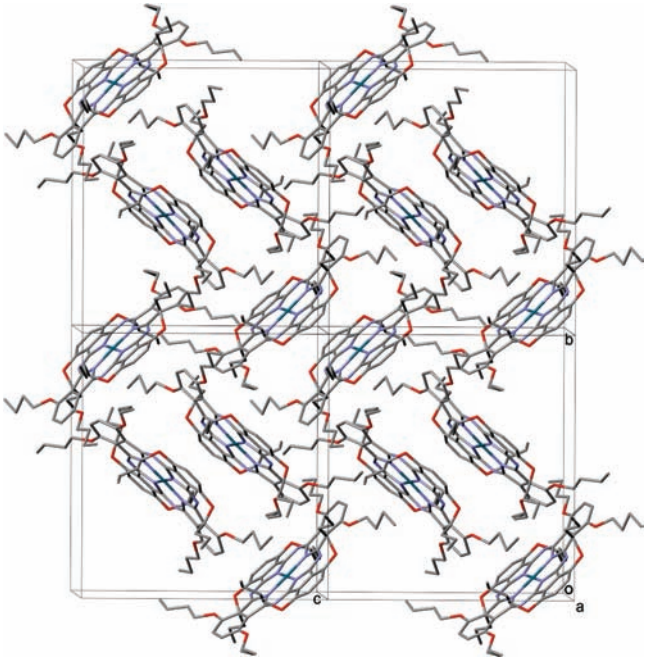

Figure 2. Crystal packing of $PdPc(OBu)_8$ shown approximately along the a axis. Hydrogen atoms and disorder have been omitted for clarity.

(39) Liu, W.; Lee, C. H.; Chan, H. S.; Mak, T. C. W.; Ng, D. K. P. *Eur. J. Inorg. Chem.* **2004**, 286.
(40) Brown, C. J. *J. Chem. Soc. A* **1968**, 2488.

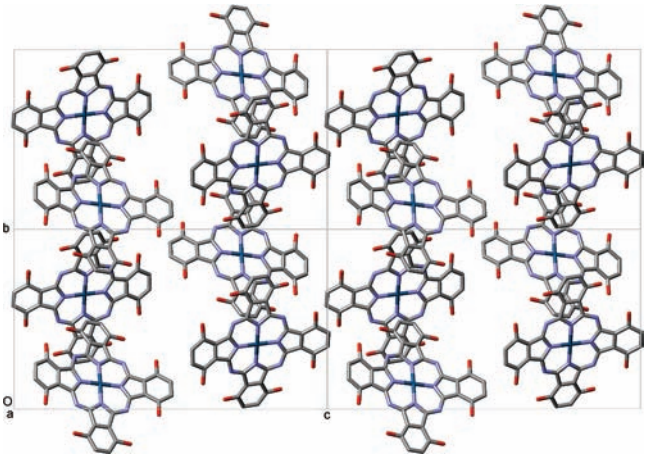

Figure 3. Crystal packing of $PtPc(OBu)_8$ viewed along the *a* axis. Hydrogen atoms and butyl chains have been omitted for clarity.

163.2°; C51A···N3^{ii}, 3.464(10) Å; H511···N3^{ii}, 2.53 Å; C51A−H511···N3^{ii}, 162.5° (symmetry codes: (i) = $1 - x$, $-0.5 + y$, $0.5 - z$; (ii) = x, $0.5 - y$, $-0.5 + z$).

In the crystal structure of $PtPc(OBu)_8$, the molecules are arranged into zigzag ribbons along the *b* axis (Figure 3) with the mean planes of adjacent macrocycles forming a dihedral angle of 52.65(7)°. No intermolecular hydrogen bonds or $\pi-\pi$ stacking interactions are observed.

C. UV−vis and NIR Absorption Spectra. The normalized UV−vis absorption spectra of $PdPc(OBu)_8$ and $PtPc(OBu)_8$ in benzene and dimethylformamide (DMF) solution are displayed in Figure 4 where those of the nickel analogue are also reported, for comparison purpose.

The overlaid spectra in Figure 4 show that the complexes of the triad share similar spectral features, that is, a very intense Q(0,0) band in the 710−750 nm region with a vibrational progression to the blue, a weaker B band system around 300−330 nm, and a moderately intense and broad absorption in between, at around 437−450 nm, which is characteristic of α-alkoxysubstituted phthalocyanines.[4,6,41] The Q-band system experiences a blue shift going from Ni through Pd to Pt, in line with the trend observed in virtually all tetrapyrrolic complexes of this triad.[42] Furthermore, the B band system profile varies significantly with the central metal and the solvent. Comparing the overlaid spectra of the complexes of the triad in benzene and DMF, it is apparent that the major effect of the increased polarity of the solvent consists in the red shift of the main spectral features, which is particularly pronounced (~ 15 nm) for the Q-band system.

$PdPc(OBu)_8$ and $PtPc(OBu)_8$ also exhibit weak NIR absorptions, both in benzene and DMF (see Figure 5).

In benzene the Pd(II) and Pt(II) complexes show a distinct absorption at 1091 nm ($\varepsilon \approx 50$ M^{-1} cm^{-1}) and 1028 nm ($\varepsilon \approx 100$ M^{-1} cm^{-1}), respectively, followed by a very broad absorption to the blue. In DMF the NIR absorptions decrease in intensity, particularly in the case of the Pd complex. In the Pt complex the hypochromicity of the NIR band is associated with a sizable red shift.

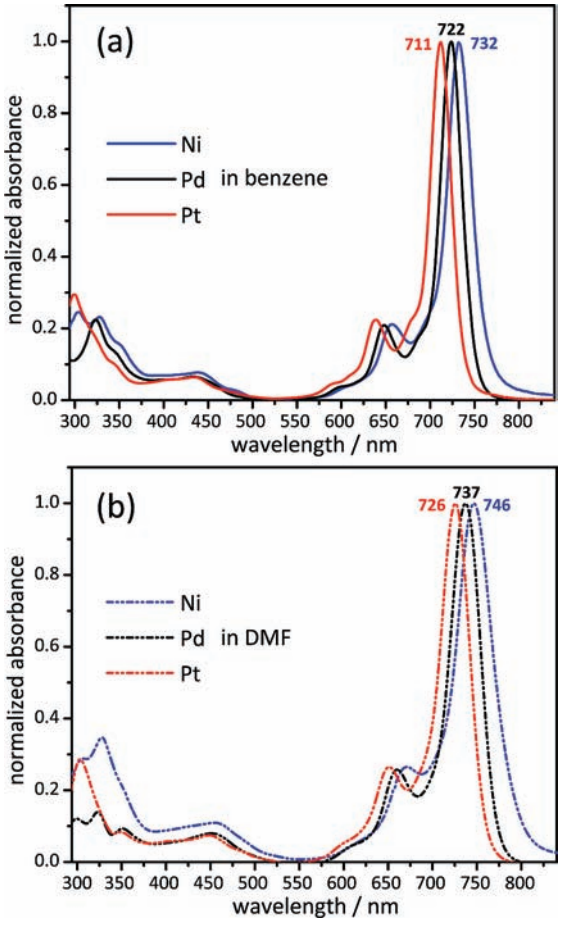

Figure 4. Normalized UV−vis absorption spectra of $MPc(OBu)_8$ (M = Ni, Pd, Pt) at room-temperature in (a) benzene and (b) DMF.

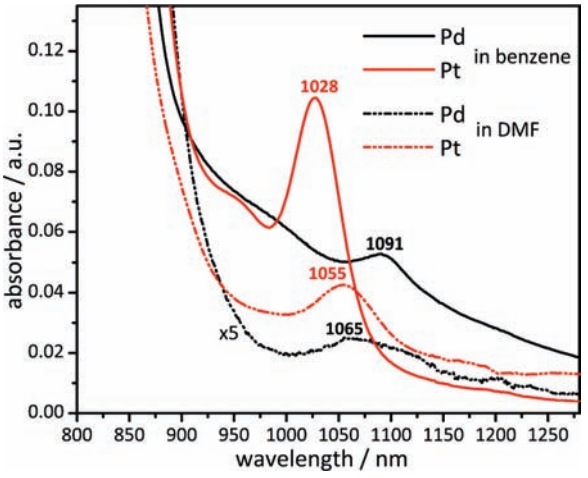

Figure 5. NIR absorption spectra of 1.7 mM $MPc(OBu)_8$ (M = Pd, Pt) in benzene and DMF, at room-temperature.

D. Steady-State Absorption and Luminescence Experiments. The normalized absorbance and fluorescence spectra of the Pd and Pt complexes in the Q-band region are brought together in Figure 6, which also displays the phosphorescence spectra in the NIR region. The most relevant data obtained from steady-state absorption and emission experiments are summarized in Table 2.

In benzene both compounds exhibit weak fluorescence from the Q(0,0) band with maxima at 734 (Pd) and

(41) Bian, Y.; Li, L.; Dou, J.; Cheng, D. Y. Y.; Li, R.; Ma, C.; Ng, D. K. P.; Kobayashi, N.; Jiang, J. *Inorg. Chem.* **2004**, *42*, 7539.

(42) Gouterman, M. The Porphyrins. In *The Porphyrins*; Dolphin, D., Ed.; Academic Press: New York, 1978; Vol. *3*; Chapter 1.

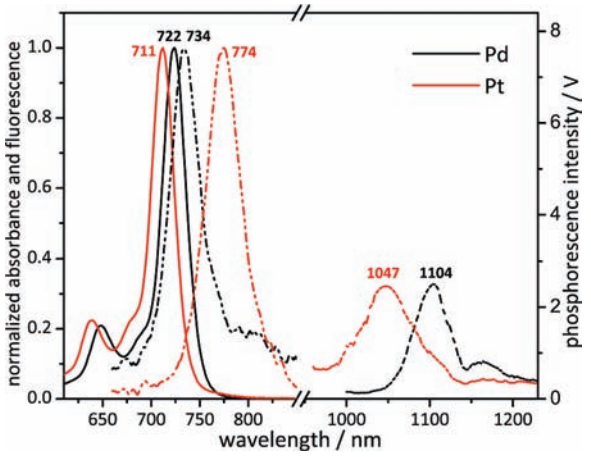

Figure 6. Absorption (solid lines), fluorescence (dashed lines) and phosphorescence (dotted lines) spectra of $PdPc(OBu)_8$ (black) and $PtPc(OBu)_8$ (red) at 295 K. The absorption and fluorescence spectra are normalized to an arbitrary maximum of 1.0. The absorption spectra were taken in benzene. The fluorescence spectra were obtained in air-saturated benzene, and the excitation wavelength was 645 nm. The phosphorescence spectra were obtained in Ar-saturated benzene, and the excitation wavelength was 488 nm.

774 nm (Pt). The agreement with previously published absorption and fluorescence steady-state spectra of $PdPc(OBu)_8$[3] is excellent. The fluorescence quantum yield measured for $PdPc(OBu)_8$ was 8×10^{-4}, that is, comparable with the $\sim 5 \times 10^{-4}$ value reported for the unsubstituted analogue, PdPc.[43] The Pt complex showed a stronger fluorescence signal with quantum yield of 2×10^{-3}. As apparent from Figure 6, in benzene, the fluorescence emission maximum occurs in the Pt complex at a much longer wavelength than in the Pd complex to the effect that the Stokes shift is significantly larger in the former than in the latter (1145 vs 226 cm^{-1}, see Table 2). Interestingly, going from benzene to DMF the Stokes shift in the Pt complex reduces to 230 cm^{-1} whereas that of the Pd complex increases to 342 cm^{-1}. Stokes shifts comparable to that shown by $PtPc(OBu)_8$ in benzene were measured by Kobayashi et al.[4] for $H_2Pc(OBu)_8$ (1130 cm^{-1}) and $ZnPc(OBu)_8$ (1150 cm^{-1}) in THF. For the same compounds Rihter et al.[3] measured in benzene much smaller Stokes shifts (270 cm^{-1} in both cases) than those obtained by Kobayashi et al.,[4] in THF. All together these data indicate that, depending on the central metal, the increase of the solvent polarity induces either an increase or a decrease of the Stokes shift. We will return to this point when discussing the TDDFT results for the emitting S_1 state.

Besides fluorescence emission, the deaerated solutions of $PdPc(OBu)_8$ and $PtPc(OBu)_8$ exhibit an additional emission in the near-infrared. This emission is assigned to phosphorescence because its intensity decreases substantially when the solution is saturated with O_2. In Ar-saturated benzene the $T_1(0,0)$ emission maxima are at 1104 and 1047 nm for the palladium and platinum compounds, respectively (see Figure 6 and Table 2) indicating that the S_1-T_1 and T_1-S_0 energy gaps in $PdPc(OBu)_8$ are larger than in $PtPc(OBu)_8$. The triplet quantum yield, Φ_T, in the Pt complex is significantly lower (70%) than in the Pd complex. This is in contrast with the "energy gap law", but in line with the $T_1 \rightarrow S_0$ ISC process being more efficient in the heavier element phthalocyanine.

Table 2. Absorption and Emission Data for $Pd(OBu)_8$ and $Pt(OBu)_8$ at 295 K

	Q(0,0)	fluorescence			phosphorescence
	λ_{max} (nm)[a]	λ_{max} (nm)[b]	Φ_F[c]	Stokes shift (cm^{-1})[b]	λ_{max} (nm)[d]
Pd	722/737	734/756	0.0008	226/342	1104
Pt	711/726	774/749	0.002	1145/423	1047

[a] Taken in benzene/DMF. [b] Taken in air-saturated benzene/DMF. [c] Measured in air-saturated benzene. [d] Taken in Ar-saturated benzene.

E. Transient Absorption Experiments: Spectral Observations and Dynamic Properties. The triplet state of $PdPc(OBu)_8$ is well characterized as this compound was considered to have potential for use in PDT,[3] but the excited state dynamics on the picosecond time scale has never been reported. On the other hand, the excited state dynamics of $PtPc(OBu)_8$ has never been investigated.

$PdPc(OBu)_8$ and $PtPc(OBu)_8$ show similar transient absorption features on the femtosecond and nanosecond time scale. Evolution of the transient absorption signals of the Pd and Pt complexes in benzene are displayed in Figure 7 and Figure S3 in the Supporting Information, respectively. The spectral signatures of the ultrafast transient absorption spectra observed promptly (1.8 ps) after 650 nm excitation (Figure 7a) closely resemble the $S_1 \rightarrow S_n$ spectra reported for a number of metallophthalocyanines,[3,6,23,25,44] namely, a broad positive absorption with maximum at 620 nm and two negative bands at 655 and 730 nm because of ground state depopulation. By analogy to assignments made for other metallophthalocyanines,[3,6,23,25,44] the first observed transient in the two studied complexes is assigned to $S_1 \rightarrow S_n$ transitions.

During the first 50 ps, a small rise of the positive absorption band at 620 nm and concomitant growth of the signals in the region of the ground state bleaching could be observed for $PdPc(OBu)_8$; two isosbestic points at 515 and 690 nm connected these kinetic features. After that, no changes in the transient absorption spectra could be detected during the time window of the ultrafast spectrometer ($\sim$1.6 ns).

In $PtPc(OBu)_8$ similar spectral changes occurred during the first 5 ps. These changes can be attributed to $S_1 \rightarrow T_1$ crossing in the π-system. The final ultrafast transient closely resembles the nanosecond transient spectrum (Figure 7b and Figure S3b in the Supporting Information) and is identified as originating from $T_1 \rightarrow T_n$ absorption.

The nanosecond transient absorption profiles of the Pd and Pt complexes in deaerated benzene at different delay times after 355 nm excitation are shown in Figure 7b and Figure S3b in the Supporting Information, respectively. The transient spectrum at 60 ns shows positive absorption features in the 480−685 nm and 770−850 nm regions. The negative absorption bands that can be seen in the Soret (330 nm) and Q-band (730 nm) regions are assigned to ground state bleaching. The spectral signature of these absorptions resembles the last transient on the picosecond

(43) Vincett, P. S.; Voigt, E. M.; Rieckhoff, K. E. *J. Chem. Phys.* **1971**, *55*, 4131.

(44) Gunaratne, T. C.; Kennedy, V. O.; Kenney, M. E.; Rodgers, M. A. J. *J. Phys. Chem. A* **2004**, *108*, 2576.

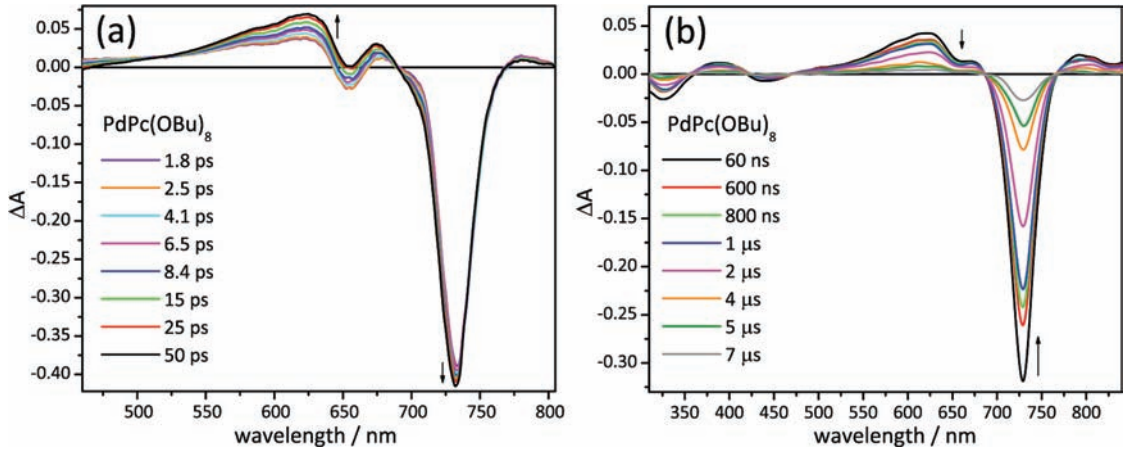

Figure 7. (a) Ultrafast transient absorption difference spectra of ~22 mM $PdPc(OBu)_8$ in benzene at different delay times after 650 nm excitation. (b) Nanosecond transient absorption difference spectra of ~6 mM $PdPc(OBu)_8$ in benzene at different delay times after 355 nm excitation. Vertical arrows indicate evolution of the transient absorption signal.

time scale assigned to the T_1 state and has similar spectral properties to those of triplet states localized on the π-system of metallophthalocyanines studied earlier.[3,23,25,44−46] These transient absorption features decayed uniformly, returning the system to the ground state. The isosbestic points at 358 nm, 420 nm, 472 nm, 685 nm, and 768 nm separate the positive and negative region of the transient spectra, indicating that the positive absorption due to the T_1 state decayed by repopulating the ground state surface.

In the femtosecond transient absorption experiments, the growth of the ground state bleaching signal and the growth of the positive absorption were fitted by a single exponential function to a non-zero baseline. Figures 8a,b display the temporal profiles of the transient absorption on the picosecond time scale taken at the absorption maxima for the Pd and Pt complexes. The lifetime of the formation of the triplet state via intersystem crossing was different for the two complexes, namely, 11.2 ps for $PdPc(OBu)_8$ and 1.31 ps for $PtPc(OBu)_8$, indicating a more efficient ISC process for the heavier element complex. Figures 8c,d illustrate the decay profile of the nanosecond transient absorption signal of the studied compounds at their spectral maxima. The triplet state of $PdPc(OBu)_8$ and $PtPc(OBu)_8$ decayed directly to the S_0 surface with lifetimes of 3.04 and 0.55 μs, respectively.

In the presence of oxygen, the decay of the triplet state was enhanced for both compounds indicating quenching of the T_1 state by O_2. The bimolecular rate constants for quenching of the triplet state of $PdPc(OBu)_8$ and $PtPc(OBu)_8$ in benzene by molecular oxygen were obtained by measuring the triplet state lifetimes in solutions with different oxygen concentrations. The bimolecular rate constants for oxygen quenching, $k_{T\Sigma}$, were found to be 2.84×10^9 and 4.22×10^9 M^{-1} s^{-1} for the Pd and Pt complexes, respectively. The $k_{T\Sigma}$ values indicate that the energy transfer from the metallophthalocyanine triplet state to $O_2(^3\Sigma_g^-)$ is energetically favored. The triplet state properties of the two complexes are summarized in Table 3.

(45) Aoudia, M.; Cheng, G.; Kennedy, V. O.; Kenney, M. E.; Rodgers, M. A. J. *J. Am. Chem. Soc.* **1997**, *119*, 6029.
(46) Spikes, J. D.; Van Lier, J. E.; Bommer, J. C. *Photochem. Photobiol. A* **1995**, *91*, 193.

F. Quantumm Chemical Calculations. Molecular Structure. Gas-phase unconstrained geometry optimization was performed, at the DFT/B3LYP/def2-TZVP level, for the palladium and platinum α-octamethoxyphthalocyanine model complexes and, for comparison purpose, for the nickel analogue, starting from the macrocycle crystal structure of the corresponding $MPc(OBu)_8$ complexes. The optimization converged in all cases to minimum energy structures of D_{2d} symmetry with the carbon atoms of the methyl groups, C_{met}, coplanar with the indole rings. Structures of D_{4h} symmetry were also explored but resulted to be saddle points with a small imaginary frequency corresponding to the saddling motion (b_{2u} symmetry). The D_{4h} structures were found to be only 0.5−1.0 kcal/mol less stable than the D_{2d} minimum structures. Previous DFT/BP86/TZ2P calculations on $NiPc(OMe)_8$ also predicted a very small energy gap between the saddled and planar structure and suggested that while in the solid state the complex is "frozen" in the saddled molecular structure, in solution it can flap from one saddled conformation through the planar "maximum" to the opposite saddled structure.[6] On the basis of the present results this holds true for the heavier element complexes.

The relevant geometrical parameters computed for the $MPc(OMe)_8$ (M = Ni, Pd, Pt) model complexes are reported in Table 4 and compared to the experimental mean values. Apart from the modest ruffling of the phthalocyanine skeleton and the random displacement of the C_{but} atoms from the indole rings, which are related to packing requirements, the salient features of the solid-state molecular structures are substantially retained in the D_{2d} structures of the model compounds. In particular, the calculations account well for the sensible decrease of the saddling distortion of the macrocycle going from Ni to the heavier element complexes suggesting that the saddling distortion of the macrocycle is primarily dictated by intrinsic electronic factors, such as the necessity to minimize the steric hindrance between the lone pairs of the facing oxygen atoms while preserving an efficient metallophthalocyanine interaction. Indeed, the degree of saddling decreases with the increase of the ionic radius of the metal. The data in Table 4 show that the saddling distortion of the macrocycle is systematically underestimated theoretically. This is mainly because the degree of saddling is

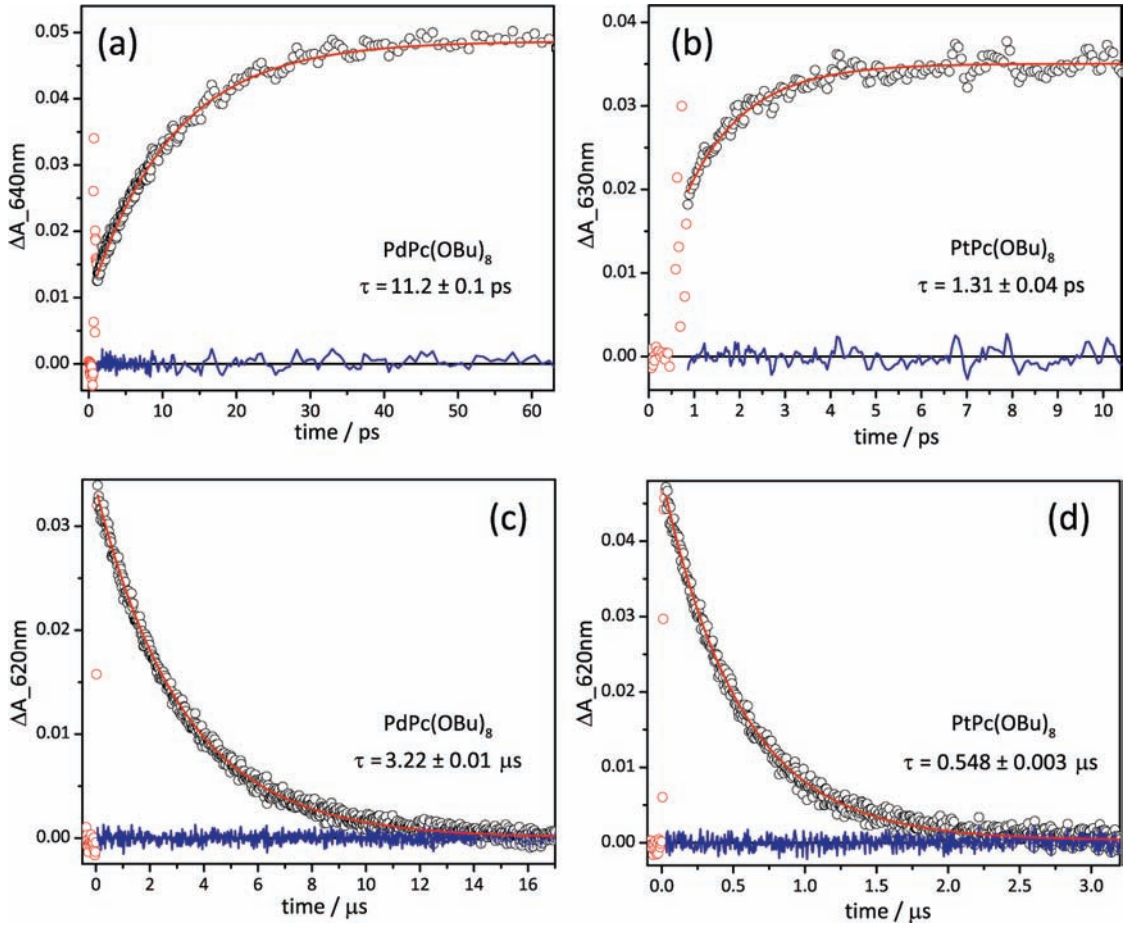

Figure 8. Kinetics profiles of the transient absorption signals of $PdPc(OBu)_8$ (a) and $PtPc(OBu)_8$ (b) in benzene. Femtosecond experiment, $\lambda_{exc} = 650$ nm; nanosecond experiment, $\lambda_{exc} = 355$ nm (in Ar-saturated benzene). Solid lines are fits to the experimental points.

Table 3. Triplet-State Properties of $Pd(OBu)_8$ and $Pt(OBu)_8$ and Triplet-State Quenching by O_2 in Benzene

	Φ_T[a]	λ_{max} (nm)	τ_{Ar}[a] (μs)	τ_{air}[b] (μs)	τ_{O2}[c] (μs)	$k_{T\Sigma}$ (M^{-1} s^{-1})
Pd	0.77	620	3.04	0.156	0.038	2.84×10^9
Pt	0.70[d]	620	0.55	0.100	0.025	4.22×10^9

[a] In Ar-saturated solutions. [b] In air-saturated solutions. [c] In O_2-saturated solutions. [d] Relative to $PdPc(OBu)_8$.

in part controlled by packing factors, which are not considered in the calculations. In addition, it should be taken into account that the magnitude of the saddling distortion is very sensitive to the level of theory (basis set, exchange-correlation functional, see ref 47 and references therein).

Consistent with the underestimation of the saddling distortion, the computed $M-N_p$ distances are slightly overestimated.

Electronic Structure. Before dealing with the excited states of the $MPc(OMe)_8$ (M = Ni, Pd, Pt) series we will briefly discuss the ground state electronic structure of these complexes, with special emphasis on the salient differences between $NiPc(OMe)_8$, whose electronic structure has been elucidated in a previous work,[6] and the heavier element complexes.

(47) Rosa, A.; Ricciardi, G.; Baerends, E. J.; Zimin, M.; Rodgers, M. A. J.; Matsumoto, S.; Ono, N. *Inorg. Chem.* **2005**, *44*, 6609.

Table 4. Selected Bond Lengths (Å), Bond Angles (deg), and Metrical Parameters Computed for $MPc(OMe)_8$ (M = Ni, Pd, Pt) Model Complexes in the Gas-phase at DFT/B3LYP/def2-TZVP Level of Theory Are Compared to the Experimental Data

	Ni		Pd		Pt	
	calc.	exp.[a]	calc.	exp.[b]	calc.	exp.[b]
$M-N_p$	1.921	1.878(4)	1.995	1.979(2)	1.997	1.951(6)
$C_\alpha-N_p$	1.373	1.376(6)	1.368	1.374(4)	1.371	1.367(10)
$C_\alpha-C_\beta$	1.454	1.455(7)	1.459	1.467(5)	1.458	1.449(11)
$C_\beta-C_\beta$	1.400	1.397(7)	1.406	1.423(5)	1.406	1.390(11)
$C_\alpha-N_b$	1.314	1.320(6)	1.319	1.324(5)	1.318	1.322(11)
C_o-O	1.355	1.361(6)	1.355	1.369(5)	1.355	1.386(15)
$\angle C_\alpha N_p C_\alpha$	107.7	107.0(4)	110.2	109.4(2)	110.2	108.7(6)
$\angle C_\alpha N_b C_\alpha$	122.5	120.1(4)	125.2	123.9(3)	125.6	122.7(7)
$O\cdots O$	3.620	3.91(2)	3.600	3.738(4)	3.590	3.789(16)
φ_{sad}	7.2	16.2(4)	3.4	7.21(5)	2.3	9.7(1)

[a] X-ray data from ref 6. [b] X-ray data, this work.

The highest occupied and lowest unoccupied one-electron levels computed for the complexes of the triad are shown in Figure 9.

The most prominent difference between $NiPc(OMe)_8$ and the heavier element analogues is the destabilization of the $M(nd_{x^2-y^2})-N_p(lp)$ σ-antibonding MO, the $30b_2$, with respect to the highest occupied molecular orbital (HOMO). This can be traced primarily to the increase of the M/N_p overlap as the diffuseness of the $M-nd_{x^2-y^2}$ orbitals increases in the order 3d < 4d < 5d. The relevant consequence of the upshift of the $M-N_p$ σ-antibonding

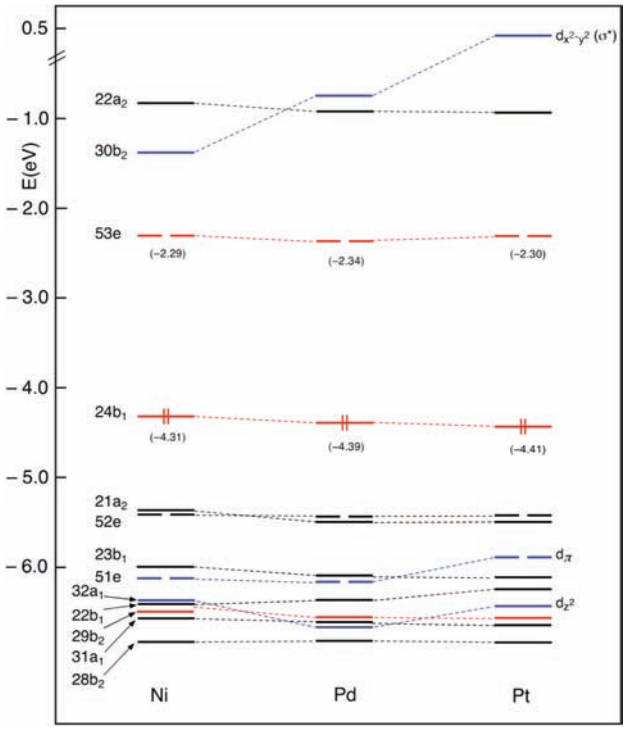

Figure 9. Energy level scheme for $MPc(OMe)_8$ (M = Ni, Pd, Pt). For the sake of clarity, for the MOs of the three complexes the same numbering has been adopted. The Gouterman MOs are printed in red. The MOs with significant metal character are printed in blue.

$30b_2$ is that the $^{1,3}LMCT(\pi,d_{x^2-y^2})$ excited states, which are central intermediates in the radiationless decay of $NiPc(OBu)_8$, are in the heavier element complexes too high in energy to provide effective routes for deactivation of the normally emissive $^{1,3}(\pi,\pi^*)$ states; $PdPc(OBu)_8$ and $PtPc(OBu)_8$ are indeeed luminescent.

As apparent from the level scheme in Figure 9, the occupied $M(nd_\pi)-N_p(2p_z)$ π-antibonding 51e, which contains a sizable metal-d_π percentage (Ni: 31%, Pd: 21%, Pt: 28%), is much less sensitive to the metal than the σ-antibonding $30b_2$. The modest energy change of the 51e along the triad results from a delicate balance between the increase of the destabilization and the increase of the diffuseness of the M−nd orbitals down the triad. The same argument holds for the $32a_1$ MO, which is basically a pure nd_{z^2} orbital with some (n+1)s contribution and small (antibonding) admixture of N_p lone pairs.

As for the ligand MOs, these show, as expected, a very modest sensitivity to the central metal. Nevertheless, the even small energy changes of some of them deserve attention because they are at the origin of the observed spectral changes along the series. This is the case of the HOMO, the G-$24b_1$ (G = Gouterman), and the two degenerate lowest unoccupied molecular orbitals (LUMOs), the G-53e. The former is slightly stabilized along the series, the LUMOs downshift from Ni to Pd and upshift from Pd to Pt, to the net effect that the HOMO−LUMO gap slightly increases down the triad. The stabilization of the HOMO along the series can be traced to the relief of π-antibonding interaction between the C_α-$2p_z$ orbitals upon expansion of the macrocycle core, which is consistent with the nodal pattern of the HOMO (see the plot of this orbital in Figure 10).

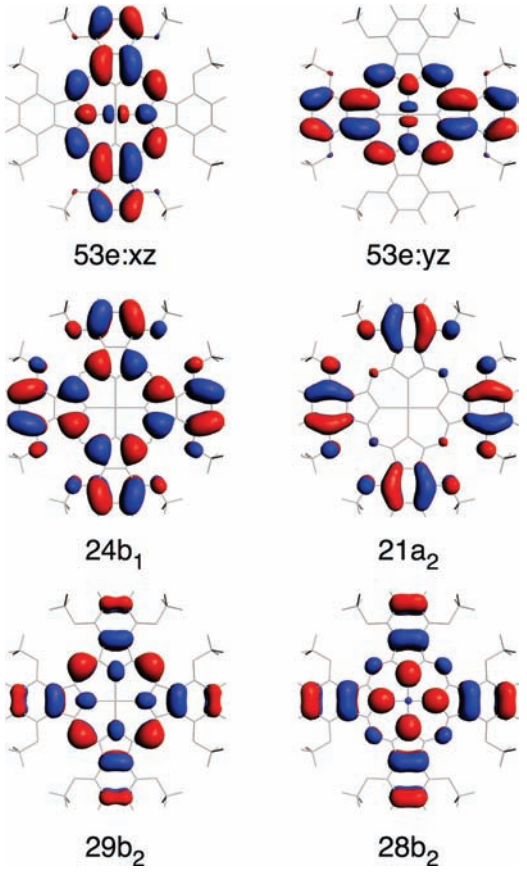

Figure 10. Relevant Kohn−Sham molecular orbitals of $PtPc(OMe)_8$.

There are counteracting effects on the position of the LUMOs along the series. On the one hand, consistent with their nodal pattern (see plots in Figure 10), the LUMOs will be stabilized upon expansion of the macrocycle. On the other hand, the antibonding mixing with the M-nd_π increases as the diffusennes of the d orbitals increases (the nd_π contribution to the LUMOs increases from 2% to 4% down the triad) leading to a destabilization of the LUMOs.

Among the ligand orbitals, worth mentioning are the $21a_2$ and the low-lying $29b_2$ and $28b_2$ MOs. The $21a_2$ is, together with the HOMO, a π orbital of the macrocycle that is strongly destabilized by antibonding with the oxygen lone pairs (see the plot of the $21a_2$ in Figure 10) and becomes the HOMO-1 in the nickel complex and the HOMO-2 in the palladium and platinum analogues. As it will be shown in the next section, transitions out of the $21a_2$ into the LUMOs are responsible for the moderately intense absorption at around 437−450 nm, which is characteristic of virtually all α-alkoxysubstituted phthalocyanines.[4,6,41] With regard to the $29b_2$ and $28b_2$ MOs, they are a mixture of the two "a_{2u}" MOs of unsubstituted phthalocyanines (see the plots of these MOs in Figure 10), whose origin and spectroscopic relevance has been theoretically elucidated in previous works.[48,49] The $29b_2$ has larger amplitude on the aza-bridges compared to the lower-lying $28b_2$ and thus can be identified as the true

(48) Rosa, A.; Ricciardi, G.; Baerends, E. J.; Van Gisbergen, S. J. A. *J. Phys. Chem. A* **2001**, *105*, 3311.
(49) Ricciardi, G.; Rosa, A.; Baerends, E. J. *J. Phys. Chem. A* **2001**, *105*, 5242.

Table 5. Vertical Excitation Energies (E_{va}) and Oscillator Stregths (f) Computed for the Spin and Symmetry Allowed Excited States of $NiPc(OMe)_8$ Contributing to the UV-vis Spectral Region

		benzene		DMF		exptl
state	composition[a] (%)	E_{va} (eV/nm)	f	E_{va} (eV/nm)	f	λ_{max} (nm)[b]
1^1E	$24b_1 \rightarrow 53e$ (96)	1.83/678	0.897	1.77/700	0.866	732/746
3^1E	$21a_2 \rightarrow 53e$ (99)	2.61/475	0.335	2.52/492	0.371	440/451
8^1E	$31a_1 \rightarrow 53e$ (85)	3.59/345	0.040	3.54/350	0.027	350/351
9^1E	$29b_2 \rightarrow 53e$ (60) $28b_2 \rightarrow 53e$ (29)	3.89/319	0.976	3.84/323	0.669	329/323
10^1E	$28b_2 \rightarrow 53e$ (59) $29b_2 \rightarrow 53e$ (15)	3.96/313	0.354	3.98/312	0.609	

[a] The composition of the excited states refers to TDDFT calculations in benzene; in DMF no significant changes in the composition of the excited states are observed. [b] In benzene/DMF solutions, this work.

"Gouterman" orbital correlating with the "a_{2u}" of the nominally planar MPcs. According to the level scheme in Figure 9, the energy gap between the $29b_2$ and $28b_2$ MOs slightly decreases on going from Ni to the heavier element phthalocyanines. This has a significant impact on the profile of the B band system (vide infra).

In benzene, and in DMF even more, both the occupied and virtual MOs are stabilized, the former somewhat less than the latter, though. The amount of the downshift of the occupied and virtual MOs is nearly the same in all members of the series. The solvent-induced electronic structure changes account well for the solvatochromism of the $MPc(OMe)_8$ (M = Ni, Pd, Pt) complexes, as explicit TDDFT calculations of the excited states will show.

Excited States and Absorption Spectra. (a). UV−vis Spectra. To provide an assignment of the UV−vis absorption spectra of the $MPc(OBu)_8$ complexes TDDFT calculations of the optically allowed singlet B_2 and E states in the energy range covered by the experimental spectra have been performed, both in benzene and DMF solutions. The computed excitation energies and oscillator strengths are gathered in Tables 5−7. The singlet B_2 states are not included in the tables because their oscillator strengths were lower than 0.01 in the investigated energy range and therefore not relevant to the interpretation of the main spectral features.

According to the TDDFT results, regardless of the solvent, in all complexes the intense Q-band is accounted for by the lowest singlet E state, which originates from transitions out of the HOMO to the two degenerate LUMOs. Consistent with the increase of the HOMO/LUMOs gap on going from Ni to the heavier element phthalocyanines, the excitation energy of the 1^1E state shifts to the blue down the triad, in perfect agreement with the experiment. Consistent with the decrease of the HOMO/LUMOs gap on going from benzene to DMF, in all complexes the 1^1E state is computed at a lower energy in the DMF solvent than in benzene, thus reproducing the observed shift of the Q-band to longer wavelengths on increasing the solvent polarity. The next state with sizable intensity, namely, the 3^1E in the nickel complex and the 2^1E in the Pd and Pt analogues, is an almost pure $21a_2 \rightarrow 53e$ state. On the basis of the energy and oscillator strength this state can be unambiguously assigned to the moderately intense and broad band

Table 6. Vertical Excitation Energies (E_{va}) and Oscillator Stregths (f) Computed for the Spin and Symmetry Allowed Excited States of $PdPc(OMe)_8$ Contributing to the UV-vis Spectral Region

		benzene		DMF		exptl
state	composition[a] (%)	E_{va} (eV/nm)	f	E_{va} (eV/nm)	f	λ_{max} (nm)[b]
1^1E	$24b_1 \rightarrow 53e$ (96)	1.85/670	0.914	1.79/693	0.879	722/737
2^1E	$21a_2 \rightarrow 53e$ (99)	2.60/477	0.368	2.51/494	0.412	437/450
6^1E	$31a_1 \rightarrow 53e$ (87)	3.60/344	0.028	3.55/349	0.015	345/351
7^1E	$28b_2 \rightarrow 53e$ (60) $29b_2 \rightarrow 53e$ (33)	3.86/320	0.404	3.80/326	0.404	323/323
9^1E	$29b_2 \rightarrow 53e$ (36) $28b_2 \rightarrow 53e$ (24) $52e \rightarrow 30b_2$ (22)	3.97/312	0.832	3.97/312	0.616	-/300

[a] The composition of the excited states refers to TDDFT/ZORA calculations in benzene; in DMF the composition of the excited states is the same as in benzene except for the $7,9^1E$ excited states in which the $29b_2 \rightarrow 53e$ and $28b_2 \rightarrow 53e$ transitions enter with a reversed weight. [b] In benzene/DMF solutions, this work.

Table 7. Vertical Excitation Energies (E_{va}) and Oscillator Stregths (f) Computed for the Spin and Symmetry Allowed Excited States of $PtPc(OMe)_8$ Contributing to the UV-vis Spectral Region

		benzene		DMF		exptl
state[a]	composition[a] (%)	E_{va} (eV/nm)	f	E_{va} (eV/nm)	f	λ_{max} (nm)[b]
1^1E	$24b_1 \rightarrow 53e$ (97)	1.89/656	0.919	1.81/685	0.882	711/726
2^1E	$21a_2 \rightarrow 53e$ (99)	2.64/470	0.358	2.54/488	0.403	437/450
6^1E	$31a_1 \rightarrow 53e$ (86)	3.69/336	0.012	3.63/342	0.004	342/351
7^1E	$29b_2 \rightarrow 53e$ (62) $28b_2 \rightarrow 53e$ (25)	3.90/318	0.657	3.84/323	0.548	300/303
8^1E	$52e \rightarrow 22a_2$ (82) $28b_2 \rightarrow 53e$ (15)	4.00/310	0.135	3.97/312	0.126	
9^1E	$28b_2 \rightarrow 53e$ (42) $29b_2 \rightarrow 53e$ (17)	4.11/302	0.326	4.15/299	0.387	

[a] The composition of the excited states refers to TDDFT calculations in benzene; in DMF no significant changes in the composition of the excited states are observed. [b] In benzene/DMF solutions, this work.

appearing in the absorption spectra of the investigated complexes at around 437−440 nm in benzene and 445−450 nm in DMF solution. This assignement confirms the previous assignment by Kobayashi et al.[4] based on Pariser−Parr−Pople (PPP) semiempirical calculations and is in accord with magnetic circular dicroism (MCD) spectra showing a Faraday A term for this band, which is, as mentioned above, characteristic of α-alkoxysubstituted phthalocyanines.[4,6,41] We note in passing that previous TDDFT/BP86 calculations on $NiPc(OMe)_8$ located the 3^1E state at much lower energy than the present TDDFT/B3LYP calculations leading to the tentative assignment of this state to the blue tail of the Q-band system.[6,50] The discrepancy between the two functionals can be traced to the well-known CT problem of TDDFT.[11,51−53] Indeed, in all three complexes, the excited state in question has appreciable intramolecular charge transfer (CT) character as it involves a transition from an MO largely localized on the benzene rings, the $21a_2$, into the highly delocalized 53e (see the plots of these

(50) Soldatova, A. V.; Kim, K.; Peng, X.; Rosa, A.; Ricciardi, G.; Kenney, M. E.; Rodgers, M. A. J. *Inorg. Chem.* **2007**, *46*, 2080.
(51) Dreuw, A.; Weisman, J. L.; Head-Gordon, M. *J. Chem. Phys.* **2003**, *119*, 2943.
(52) Dreuw, A.; Head-Gordon, M. *J. Am. Chem. Soc.* **2004**, *126*, 4007.
(53) Gritsenko, O.; Baerends, E. J. *J. Chem. Phys.* **2004**, *112*, 655.

Table 8. Vertical Excitation Energies (E_{va}) and Oscillator Strengths (in Parentheses) Computed for the Lowest Excited States of $PdPc(OMe)_8$ at SR- ZORA and ASO-ZORA TDDFT Level of Theory

	benzene		DMF		exptl
state	E_{va}[a]	dominant states	E_{va}[a]	dominant states	λ_{max}[b] (nm)
			SR-ZORA		
1^3E	1.152/1076		1.090/1137		
1^1E	1.850/670 (0.911)		1.787/694 (0.877)		
			ASO-ZORA		
$1B_1$	1.148/1080	1^3E (100%)	1.086/1142	1^3E (100%)	
$1B_2$	1.148/1080 (9.62×10^{-11})	1^3E (100%)	1.086/1142 (5.32×10^{-11})	1^3E (100%)	
1E	1.152/1076 (2.20×10^{-5})	1^3E (100%)	1.090/1137 (2.00×10^{-5})	1^3E (100%)	1091/~1065
$1A_1$	1.157/1072	1^3E (100%)	1.094/1133	1^3E (100%)	
$1A_2$	1.156/1073	1^3E (~100%)	1.094/1133	1^3E (~100%)	
2E	1.851/670 (0.911)	1^1E (100%)	1.787/694 (0.877)	1^1E (100%)	722/737

[a] Excitation energies in eV/nm. [b] In benzene/DMF solutions, this work.

Table 9. Vertical Excitation Energies (E_{va}) and Oscillator Strengths (in Parentheses) Computed for the Lowest Excited States of $PtPc(OMe)_8$ at SR- ZORA and ASO-ZORA TDDFT Level of Theory

	benzene		DMF		exptl
state	E_{va}[a]	dominant states	E_{va}[a]	dominant states	λ_{max}[b] (nm)
			SR-ZORA		
1^3E	1.213/1022		1.141/1087		
1^1E	1.886/657 (0.919)		1.815/683 (0.882)		
			ASO-ZORA		
$1B_1$	1.194/1038	1^3E (100%)	1.123/1104	1^3E (100%)	
$1B_2$	1.194/1038 (9.76×10^{-9})	1^3E (100%)	1.123/1104 (6.73×10^{-10})	1^3E (100%)	
1E	1.212/1023 (4.69×10^{-4})	1^3E (~100%)	1.141/1087 (4.12×10^{-4})	1^3E (~100%)	1028/1055
$1A_1$	1.232/1006	1^3E (100%)	1.160/1069	1^3E (100%)	
$1A_2$	1.232/1006	1^3E (100%)	1.160/1069	1^3E (100%)	
2E	1.886/657 (0.915)	1^1E (~100%)	1.815/683 (0.878)	1^1E (~100%)	711/726

[a] Excitation energies in eV/nm. [b] In benzene/DMF solutions, this work.

MOs in Figure 10). In the present case, just as previously seen in similar cases,[54−56] the standard local BP86 exchange-correlation functional underestimates the excitation energy, whereas a hybrid functional, even with only a 20% of nonlocal Hartree−Fock exchange, such as B3LYP, alleviates the problem. In fact, the energy of the intramolecular CT state (the 3^1E in the nickel complex and the 2^1E in the Pd and Pt analogues) is computed correctly at TDDFT/B3LYP level (see Tables 5−7).

In the energy regime of the B band system three excited states of sizable to large intensity are computed for $NiPc(OMe)_8$ and $PdPc(OMe)_8$, four for the Pt analogue. Of these, the lowest (the 8^1E in the nickel complex and the 6^1E in the Pd and Pt analogues) accounts for the shoulder appearing in the red tail of the B band. The observed energy trend of this shoulder along the triad is nicely reproduced theoretically, both in benzene and DMF.

Most of the intensity of the B band is accounted for by the higher-lying, nearly degenerate excited states, which are computed in very close proximity to the B band maximum. As these states, save for the 8^1E of the Pt complex, which is dominated by the $52e \rightarrow 22a_2$ $\pi \rightarrow \pi^*$ transition, consist of the same two transitions, namely, the intense Gouterman $29b_2 \rightarrow 53e$ and the rather weak $28b_2 \rightarrow 53e$, with weights varying from one compound to another, their relative intensities are quite different in the three complexes.

(b). NIR Spectra. To assign the NIR absorptions of $PdPc(OBu)_8$ and $PtPc(OBu)_8$ we have performed approximate spin−orbit ZORA TDDFT calculations of the lowest excited states of the corresponding model complexes. The excitation energies and oscillator strengths computed for the excited states up to 2.0 eV are listed in Tables 8 and 9 along with the experimental data for comparison. The components of each double-group excited state in terms of singlet and triplet single-group excited states are also listed in the tables. The SR-ZORA TDDFT results indicate that only one excited state, the 1^3E (π,π^*), lies vertically below the state accounting for the Q-band, the 1^1E (π,π^*). When spin−orbit coupling is included, six double-group excited states are obtained, two of which, the 1E and 2E, are doubly degenerate. The latter is composed (almost) entirely of the 1^1E, and its energy and oscillator strength are, within the limits of the reported figures, the same as those computed for the single-group 1^1E (π,π^*) state. The lower-lying double-group states are all dominated by the 1^3E (π,π^*) state, the 1^1E state contributing very little, if any, to these states.

(54) De Luca, G.; Romeo, A.; Monsù Scolaro, L.; Ricciardi, G.; Rosa, A. *Inorg. Chem.* **2007**, *46*, 5979.
(55) De Luca, G.; Romeo, A.; Monsù Scolaro, L.; Ricciardi, G.; Rosa, A. *Inorg. Chem.* **2009**, *48*, 8493.
(56) Donzello, M. P.; Ercolani, C.; Cai, X.; Kadish, K. M.; Ricciardi, G.; Rosa, A. *Inorg. Chem.* **2009**, *48*, 9890.

Table 10. Vertical Emission Energies (E_{ve}) and Oscillator Strengths (in Parentheses) of the Lowest Excited States of $PdPc(OMe)_8$ Computed at the Optimized Geometry of the Lowest Singlet Excited State, 1^1B_1

	benzene		DMF		exptl
state	E_{ve}[a]	dominant states	E_{ve}[a]	dominant states	λ_{max}[b] (nm)
			SR-ZORA		
1^3B_1	1.014/1223		0.953/1301		
1^3B_2	1.239/1001		1.179/1052		
1^1B_1	1.746/710 (0.443)		1.684/736 (0.420)		
1^1B_2	1.895/654 (0.453)		1.836/675 (0.439)		
			ASO-ZORA		
$1A_1$	1.014/1223 (3.11×10^{-15})	1^3B_1 (~100%)	0.953/1301 (2.67×10^{-15})	1^3B_1 (~100%)	
$1A_2$	1.014/1223	1^3B_1 (~100%)	0.953/1301	1^3B_1 (~100%)	
$1B_2$	1.014/1223 (7.14×10^{-6})	1^3B_1 (100%)	0.953/1301 (6.59×10^{-6})	1^3B_1 (100%)	
$1B_1$	1.239/1001 (1.92×10^{-5})	1^3B_2 (100%)	1.179/1052 (1.73×10^{-5})	1^3B_2 (100%)	
$2A_1$	1.239/1001 (9.61×10^{-16})	1^3B_2 (~100%)	1.179/1052 (8.01×10^{-16})	1^3B_2 (~100%)	
$2A_2$	1.239/1001	1^3B_2 (~100%)	1.179/1052	1^3B_2 (~100%)	
$2B_1$	1.746/710 (0.442)	1^1B_1 (100%)	1.684/736 (0.420)	1^1B_1 (100%)	734/756
$2B_2$	1.895/654 (0.453)	1^1B_2 (100%)	1.836/675 (0.439)	1^1B_2 (100%)	

[a] Energies in eV/nm. [b] In benzene/DMF solutions, this work.

This is not surprising in view of the dominant $\pi\pi^*$ character of the $1^{1,3}E$ states (the metal d_π contribution to the π^* MO is very low, especially in the palladium complex) and their quite large energy separation. According to the double-group excitation energies, in benzene the total zero field splitting (ZFS) of the 1^3E (π,π^*) state because of spin−orbital coupling is of 306 cm^{-1} in the Pt complex and 73 cm^{-1} in the Pd complex. Only slightly smaller ZFS values are computed in DMF. The ASO-ZORA TDDFT results for the triplet sublevels clearly indicate that the intensity of the NIR absorption mainly comes from transition to the dipole-allowed 1E state, the other states being symmetry forbidden ($1B_1$, $1A_1$, and $1A_2$) or with very low oscillator strength ($1B_2$). The experimental band maxima of the two complexes are well reproduced theoretically, both in benzene and in DMF solutions. Moreover, the observed hypochromicity of the NIR absorption on going from Pt to Pd and from benzene to DMF are accounted for by the oscillator strength computed for the 1E state.

Emission Spectra: Insights from Theory. Steady-state luminescence and transient absorption experiments strongly suggest that fluorescence and phosphorescence emissions occur from the S_1 and T_1 π,π^* states, respectively, the latter being directly populated, through ISC, from the former. To gain further insight into the emission properties and the S_1-T_1 ISC process the low-lying excited states of the investigated complexes were computed at the TDDFT/B3LYP/def2-TZVP optimized geometry of the lowest singlet and triplet excited states, the $1^1E(\pi,\pi^*)$ and $1^3E(\pi,\pi^*)$. These states are doubly degenerate and are expected to Jahn−Teller (J-T) distort into a D_2 or C_{2v} structure along the b_1 or b_2 active modes, respectively.[57] The geometry search for the singlet and triplet states led to a structure with C_{2v} symmetry. The resulting $1^{1,3}B_1$ electronic states show only a minor geometrical relaxation, particularly in the case of the platinum complex, as can be inferred from the relevant structural parameters gathered in Table S4 in the Supporting Information.

(57) Bersuker, I. B. *Chem. Rev.* **2001**, *101*, 1067.

The energies and oscillator strengths of the low-lying excited states of the palladium and platinum model complexes computed in benzene and DMF solutions at the gas-phase optimized geometry of the 1^1B_1 state are reported in Tables 10 and 11. As can be seen in Table 10, the SR-ZORA emission energies computed in benzene and DMF for the 1^1B_1 state of $PdPc(OMe)_8$ compare well with the experimental fluorescence data. The observed red shift of the emission band going from benzene to DMF is also reproduced theoretically. The ASO-ZORA results show that the fluorescent 1^1B_1 state does not undergo spin−orbit mixing with either higher-lying or lower-lying singlet and triplet states, the double-group $2B_1$ being entirely composed of the $1^1B_1(\pi,\pi^*)$ state.

As for the fluorescence emission of the Pt complex, the agreement between theory and experiment is excellent in DMF, the vertical emission energy of the 1^1B_1 state being computed only 24 nm to the blue of the fluorescence band maximum. In benzene the agreement between theory and experiment, however, is not as good as in DMF. In the less polar solvent we compute for the 1^1B_1 state a vertical emission energy of 1.781 eV (696 nm), a value that is 0.18 eV (78 nm) higher than the experimental band maximum. Such a discrepancy between theory and experiment still holds when spin−orbit coupling is taken into account, as can be inferred from the energy and composition of the double-group $2B_1$ state in Table 11. Therefore, the anomalously large Stokes shift observed in benzene cannot be traced to spin−orbit coupling effects. A plausible explanation is that in benzene the equilibrium geometry of the S_1 state is significantly different from that of the ground state most likely because of specific interactions between the solvent and the peripheral butyl chains. Unfortunately, the calculations are unable to model these effects because the geometry of the S_1 state could only be computed in vacuo. The occurrence of specific interactions between $PtPc(OMe)_8$ in its S_1 excited state and benzene molecules was verified by ad hoc calculations and ruled out on the basis of the obtained results.

Turning to the ASO-ZORA TDDFT results, it is gratifying that the electric dipole radiative lifetime, τ_{rad},

Table 11. Vertical Emission Energies (E_{ve}) and Oscillator Strengths (in Parentheses) of the Lowest Excited States of $PtPc(OMe)_8$ Computed at the Optimized Geometry of the Lowest Singlet Excited State, 1^1B_1

	benzene		DMF		exptl
state	E_{ve}[a]	dominant states	E_{ve}[a]	dominant states	λ_{max}[b] (nm)
			SR-ZORA		
1^3B_1	1.077/1151		1.008/1230		
1^3B_2	1.293/959		1.225/1012		
1^1B_1	1.781/696 (0.446)		1.711/725 (0.421)		
1^1B_2	1.927/643 (0.456)		1.862/666 (0.441)		
			ASO-ZORA		
$1A_1$	1.076/1152 (8.14×10^{-18})	1^3B_1 (99%) 1^3B_2 (1%)	1.006/1232 (5.42×10^{-18})	1^3B_1 (99%) 1^3B_2 (1%)	
$1A_2$	1.076/1152	1^3B_1 (99%) 1^3B_2 (1%)	1.006/1232	1^3B_1 (99%) 1^3B_2 (1%)	
$1B_2$	1.077/1151 (1.52×10^{-4})	1^3B_1 (~100%)	1.008/1230 (1.36×10^{-4})	1^3B_1 (~100%)	
$1B_1$	1.292/960 (4.14×10^{-4})	1^3B_2 (~100%)	1.225/1012 (3.63×10^{-4})	1^3B_2 (~100%)	
$2A_1$	1.294/958 (3.16×10^{-18})	1^3B_2 (99%) 1^3B_1 (1%)	1.227/1010 (2.94×10^{-18})	1^3B_2 (99%) 1^3B_1 (1%)	
$2A_2$	1.294/958	1^3B_2 (99%) 1^3B_1 (1%)	1.227/1010	1^3B_2 (99%) 1^3B_1 (1%)	
$2B_1$	1.781/696 (0.445)	1^1B_1 (~100%)	1.712/724 (0.421)	1^1B_1 (~100%)	774/749
$2B_2$	1.928/643 (0.456)	1^1B_2 (~100%)	1.862/666 (0.441)	1^1B_2 (~100%)	

[a] Excitation energies in eV/nm. [b] In benzene/DMF solutions, this work.

Table 12. Vertical Emission Energies (E_{ve}) and Oscillator Strengths (in Parentheses) from the Lowest Triplet Minimum to the Ground State Computed for $MPc(OMe)_8$ (M = Pd, Pt) in Benzene Solution Are Compared to the Experimental Data[a]

	Pd		Pt		exptl
state	E_{ve}[a]	dominant states	E_{ve}[a]	dominant states	λ_{max}[b] (nm)
			SR-ZORA		
1^3B_1	0.923/1343		1.007/1231		
			ASO-ZORA		
$1A_2$	0.923/1343	1^3B_1 (~100%)	1.006/1232	1^3B_1 (99%) 1^3B_2 (1%)	
$1A_1$	0.923/1343 (3.9×10^{-10})	1^3B_1 (~100%)	1.006/1232 (3.9×10^{-16})	1^3B_1 (99%) 1^3B_2 (1%)	
$1B_2$	0.923/1343 (5.1×10^{-6})	1^3B_1 (100%)	1.007/1231 (2.1×10^{-4})	1^3B_1 (~100%)	1104/1047

[a] Excitation energies in eV/nm. [b] Pd/Pt phosphorescence emission data in benzene solution, this work.

computed for the fluorescent $2B_1(1^1B_1)$ state, namely, 17 and 16 ns for Pd and Pt, respectively, is in reasonable agreement with the intrinsic fluorescence lifetime, τ_F, estimated by the Strickler−Berg equation to be 4.3 ns for both complexes. We note in passing that the fluorescence lifetimes are sufficiently large with respect to the non-radiative (ISC) deactivation, which occurs in the picosecond time scale, to justify the observed fluorescence emission.

The occurrence of a fast $S_1 \rightarrow T_1$ ISC process is accounted for by the calculations showing that at the optimized geometry of the emitting $1^1B_1(\pi,\pi^*)$ excited state only two states, the $1^3B_1(\pi,\pi^*)$ and $1^3B_2(\pi,\pi^*)$, lie vertically below the $1^1B_1(\pi,\pi^*)$. ASO-ZORA TDDFT results indicate that these singlet and triplet $\pi\pi^*$ states do not mix significantly, and in both complexes the 1^3B_2 sublevels lie vertically 0.5 eV or so below the minimum of the $S_1(2B_1)$ state (see Tables 10 and 11), thus opening a route for a fast non-radiative decay toward the lower lying set of 1^3B_1 sublevels. Taking into account that the actual energy separation between the $S_1(2B_1)$ state and the 1^3B_2 sublevels in the platinum complex is significantly smaller than the computed one (the S_1 minimum is overestimated theoretically), the decrease of the ISC lifetime on going from $PdPc(OBu)_8$ to $PtPc(OBu)_8$ (11.2 vs 1.31 ps) becomes understandable.

The emission from the lowest triplet state, the 1^3B_1, to the ground state, so-called phosphorescence, is a spin-forbidden process. To describe such process, the SOC effects need to be considered. Table 12 lists the ASO-ZORA emission energies and oscillator strengths of the three 1^3B_1 sublevels. The total ZFS of the 1^3B_1 sublevels is in the Pt complex of $\sim 8\ cm^{-1}$ and less than 1 wavenumber in the Pd complex (too small to be discerned from the reported figures), in keeping with the largely $\pi\pi^*$ character of these states. Under the experimental conditions (room temperature) the triplet-sublevels are not resolved. They remain in thermal equilibrium, as judged by the single exponential decay of the triplet state. According to

the computed oscillator strengths, of the three sublevels, the $1B_2$ is expected to give most of the intensity to the emission band. The electric dipole radiative lifetime computed for this state is 5.3 ms for the Pd complex and 0.2 ms for the Pt analogue.

Turning to the ASO-ZORA emission energies, it can be noted that although the phosphorescence emission band maxima are somewhat underestimated theoretically, the observed blue shift on going from $PdPc(OBu)_8$ to $PtPc(OBu)_8$ is well reproduced.

Conclusions

The structural, optical and photophysical properties of $PdPc(OBu)_8$ and the newly synthesized $PtPc(OBu)_8$ complexes were investigated experimentally and interpreted with the aid of SR-ZORA DFT and SR-ZORA/ASO-ZORA TDDFT calculations on $MPc(OMe)_8$ model systems. The results were compared to those previously reported for the nickel analogue, in an effort to highlight the effect of the central metal on the ground and excited state properties of the group 10 transition metal α-octabutoxyphthalocyanines. At variance with $NiPc(OBu)_8$[6] where the macrocycle assumes a remarkable saddle conformation, with the indole rings tilted alternately up and down, almost as rigid bodies, $PdPc(OBu)_8$ and $PtPc(OBu)_8$ show a modest and less regular saddling distortion of the macrocycle with the vertical tilting varying significantly from an indole to another.

The complexes share with the nickel analogue similar UV−vis spectra, with the Q-band system experiencing a blue shift down the group, as observed in virtually all tetrapyrrolic complexes of this triad.[42] Moreover, the absorption spectra show a systematic red shift in response to the increase of the solvent dielectric constant. TDDFT calculations were able to provide an unambiguous assignment of the main spectral features, as well as to account for their solvatochromism. The observed blue shift of the Q-band on going from Ni through Pd to Pt is interpreted on the basis of the metal induced electronic structure changes along the series.

Unlike $NiPc(OBu)_8$, $PdPc(OBu)_8$ and $PtPc(OBu)_8$ exhibit a weak but distinct NIR absorption. This is assigned by ASO-ZORA TDDFT calculations to the transition to the double-group 1E state, which is dominated by the lowest single-group ^3E (π,π^*) state.

Both compounds exhibit rather weak fluorescence from the Q(0,0) band with solvent and metal dependent Stokes shifts. While in DMF the Stokes shift in both complexes is comparably small (< 350 cm^{-1}), in benzene the Stokes shift of the Pt complex is significantly larger than that of the Pd analogue (1145 vs 226 cm^{-1}).

Besides fluorescence, the Pd and Pt complexes exhibit strong phosphorescence emission in deaerated benzene solutions, at 1104 and 1047 nm, respectively. Transient absorption experiments suggest that fluorescence and phosphorescence emissions occur from the $S_1(\pi,\pi^*)$ and $T_1(\pi,\pi^*)$ states, respectively, the latter being directly populated, through ISC, from the former. The lifetime of the formation of the triplet state via intersystem crossing was 11.2 ps for $PdPc(OBu)_8$ and 1.31 ps for $PtPc(OBu)_8$. In turn, the triplet state decayed directly to the S_0 surface with lifetimes of 3.04 and 0.55 μs for Pd and Pt, respectively.

In the presence of oxygen, the decay of the triplet state was enhanced for both compounds indicating quenching of the T_1 state by O_2.

Futher insight into the emission properties and the S_1-T_1 ISC process was obtained from SR-ZORA and ASO-ZORA TDDFT calculations of the low-lying excited states of the model complexes at the optimized geometries of the lowest singlet and triplet excited states, the $1^{1,3}E(\pi,\pi^*)$. These states are doubly degenerate and relax, upon a C_{2v} J-T distortion, into the corresponding $1^{1,3}B_1$ states.

The fluorescence band maxima as well as their solvatochromism are generally accounted for by the calculations, although the "anomalously" large Stokes shift observed for the platinum complex in benzene is somewhat underestimated even when spin−orbit coupling effects are taken into account. The calculations account well for the experimental observation of a direct and fast decay of the $S_1(\pi,\pi^*)$ state to the $T_1(\pi,\pi^*)$ state through ISC.

The ASO-ZORA emission energies and oscillator strengths computed for the three 1^3B_1 sublevels suggest that of these, the double-group $1B_2$ gives most of the intensity to the phosphorescence emission band. Although the phosphorescence emission band maxima are somewhat underestimated theoretically, the observed blue shift on going from Pd to Pt is well reproduced. The total ZFS of the 1^3B_1 sublevels is in the Pt complex of $\sim$8 cm^{-1} and less than 1 wavenumber in the Pd complex, in keeping with the dominant $\pi\pi^*$ character of the emitting state. Owing to their triplet properties, $PdPc(OBu)_8$ and $PtPc(OBu)_8$ can be considered promising PDT photosensitizers and potential candidates for near-infrared light emitting diodes or near-infrared emitting probes as well.

Acknowledgment. A.R. and G.R. acknowledge financial support by the MIUR (PRIN2007, 2007XWBRR4_002) and Università della Basilicata (RIL Funds 2008). Sincere thanks are expressed to Dr. Albert Okhrimenko for measurements of emission spectra in benzene. The photophysical studies conducted at the Ohio Laboratory for Kinetic Spectrometry (BGSU) were supported in part by an instrumentation grant from Hayes Investment Foundation (Ohio Board of Regents). A.V.S. thanks the McMaster Foundation at BGSU for a predoctoral fellowship.

Supporting Information Available: ORTEP top views of $PdPc(OBu)_8$ and $PtPc(OBu)_8$ (Figures S1 and S2). Transient absorption difference spectra of $PtPc(OBu)_8$ in benzene (Figure S3). Selected bond lengths and angles for $PdPc(OBu)_8$ and $PtPc(OBu)_8$ (Tables S1 and S2). Selected bond lengths, bond angles, and metrical parameters computed for $MPc(OMe)_8$ (M = Pd, Pt) in the gas-phase, in benzene, and DMF solutions (Table S3). Selected bond lengths, bond angles, and metrical parameters computed for the lowest singlet and triplet excited states of $MPc(OMe)_8$ (M = Pd, Pt) in the gas-phase (Table S4). This material is available free of charge via the Internet at http://pubs.acs.org. Full X-ray structural information is available as an X-ray crystallographic file in CIF format. CIFs have been submitted to the Cambridge Crystallographic Data Centre (CCDC) with entry numbers CCDC 795563 and 795564 for $PdPc(OBu)_8$ and $PtPc(OBu)_8$, respectively.